ACTA METALLURGICA SLOVACA
2023, VOL. 29, NO. 3, 148-154

RESEARCH PAPER

INVESTIGATION ON MICROSTRUCTURE AND COMPRESSIVE STRENGTH OF BRAZING POROUS NICKEL TO COPPER AND STAINLESS STEEL

Ramizah Rozaimay [1], Tuan Zaharinie Tuan Zahari [1, 2], Yose Fachmi Buys [3], Zainul Huda [4], Poo Balan Ganesan [1], Tadashi Ariga [5]

[1] *Department of Mechanical Engineering, Universiti Malaya, 50603 Kuala Lumpur, Malaysia.*
[2] *Centre of Advanced Manufacturing & Material Processing (AMMP Centre), Universiti Malaya, 50603 Kuala Lumpur, Malaysia.*
[3] *Department of Mechanical Engineering, Faculty of Industrial Engineering, Universitas Pertamina, Jakarta 12220, Indonesia.*
[4] *Department of Materials Engineering, King Abdulaziz University, Jeddah 21589, Saudi Arabia.*
[5] *Department of Materials Science, School of Engineering, Tokai University, Kanagawa 259-1292, Japan.*

*Corresponding author: tzaharinie@um.edu.my, tel.: +60379675266, Department of Mechanical Engineering, Universiti Malaya, 50603 Kuala Lumpur, Malaysia

Received: 08.07.2023
Accepted: 05.09.2023

ABSTRACT

This paper investigates the effects of brazing temperatures on the microstructure and compressive strength for brazing porous nickel (Ni) to copper and stainless steel 304 using VZ2250 as the brazing filler metal (BFM). A high vacuum furnace is used to braze the samples. Three (3) different brazing process parameters (680°C/5 min, 710°C/5 min, and 740°C/5 min) were set with a heating rate and cooling rate of 10°C/min, respectively. The characteristics of the joint interface have been investigated to evaluate the performance of the brazed samples by use of scanning electron microscope (SEM), energy-dispersive X-Ray spectroscope (EDS), X-Ray diffractometer (XRD), and Instron Universal Testing machine (for compressive strength testing). The data obtained has been quantitively analyzed to confirm the diffusion of the BFM during the brazing process. It has been found that the diffusion process resulted in an increase in the rigidity of the porous Ni. The compressive strength tests for the brazed Cu/Porous Ni/SS304 joint showed that the maximum compressive strength can be achieved for brazing at 680°C/5 min. The highest compressive strength value has been justified by quantitative analysis of the microstructural data. It has been proved that the VZ2250 BFM effectively diffused into the porous Ni at the brazing temperature of 680°C; brittle phases (Cu_3P and Cu_6Sn_5) were detected at the brazed Interface 1, whereas $MnNi_3$ phase was observed at the brazed Interface 2.

Keywords: Porous Nickel, Nickel Foam, Brazing, Copper, Stainless Steel, Compressive Strength

INTRODUCTION

The application of heat exchangers, in industrial processes (especially in oil and gas production), ensures high productivity. Oil and gas production are the largest-scale industrial processes requiring high heat transfer efficiency. There are various types of heat exchangers appropriate for various applications. Plate heat exchangers (PHEs) are the most commonly applied heat exchangers because it help to increase energy efficiency and mitigate fouling oil and gas production onshore and offshore [1, 2]. This is why utilizing porous metal is recommended to enhance heat transfer efficiency in PHEs. Additionally, designing new porous metal for heat exchangers has also attracted considerable interest in recent years [3]. Porous metal (nickel) (also called as nickel foam) can be used to create novel, more efficient, and compact heat exchangers. Nickel is a metal with excellent electrical conductivity, thermal stability, and corrosion resistance [4-6]. In other words, the properties of porous nickel (Ni) meet the fabrication requirement for heat exchangers.

The fabrication of PHEs, utilizing porous metal, is a challenging job since it involves the joining of base metals with porous metal. This way of fabrication is essential to ensure high thermal conduction at the interfaces. Since base metals and porous metals are dissimilar materials, an appropriate method must be adopted to create a tight bond to reduce the resistance to heat transfer at their contact [7]. Several techniques have been used to join dissimilar metals [7-10]. For instance, laser welding could be one of the techniques; however, this technique can result in high energy input to the weld metal when the bond area needs to be narrowed through bonding between base metals and porous metals. Moreover, the heat-affected one (HAZ) of the porous metal may encounter shrinkage and distortion due to the laser's high heat input; laser welding can also cause root blockage of open pores and, in time, restrains the mass flow via the porous metal [7, 11]. In addition, other techniques, such as metal inert gas (MIG) welding and tungsten inert gas (TIG) welding, are also challenging to achieve defect-free dissimilar-metals welding joints because their physical and mechanical properties differ significantly [12]. Meanwhile, the diffusion bonding of dissimilar materials can result in poor mechanical properties due to the presence of micro-voids and micro-cracks. This problem is encountered due to the mismatch of the linear expansion of the dissimilar materials [13].

In view of the limitations of welding techniques, as explained in the preceding paragraphs, brazing has been regarded as an effective technique for joining dissimilar materials because it neither distorts base metal nor porous metal [7], even at high temperatures ranging from 427°C to 1093°C [14]. Furthermore, molten brazing filler metal (BFM) eliminates gas contamination at the interface thereby significantly reducing interfacial thermal conduction loss. Based on previous research [7], the intense bonding strength between porous Ni and stainless steel can be achieved when the brazing temperature is low. This phenomenon is due to the adequate reaction of BFM with the porous Ni at this low-range temperature. However, the literature, reporting brazing of porous Ni to copper and stainless steel, is rare.

The literature gap, as mentioned in the preceding paragraph, motivated the authors to conduct research on the brazing process of joining porous Ni to copper (Cu) and stainless steel 304 (SS304). This research utilized Cu-based BFM, namely VZ2250, for brazing experiments conducted at various brazing temperatures of 680°C, 710°C, and 740°C for 5 minutes. Besides targeting to achieve a successful brazing joint, this research also focuses on investigating the effect of brazing parameters in the microstructure at the bonding joint and the rigidity of porous Ni after brazing. A lower brazing temperature is expected to have better joints than a higher brazing temperature.

MATERIAL AND METHODS

Material Preparation

The research material consisted of a commercial-purity copper (Cu) piece and a stainless steel 304 (SS304) piece as the base metals, each with dimensions: 20 mm x 20 mm x 3 mm. A porous nickel (Ni) plate having 15 PPI (pores per inch) (supplied from Japan) was cut into pieces with dimensions 10 mm x 10 mm x 11.75 mm. An optical microscope (Dino-Lite Edge, Model: AM7115 Series Digital), equipped with Dino-Capture 2.0 software, was used to determine the pore's diameter by measuring the length of the observed pores. The *Dino-Lite Edge* captures the images with a magnification of X10. Prior to brazing, both base metals were ground using silicon carbide (SiC) abrasive paper to remove the contaminated elements from the surface. VZ2250 (supplied by VACUUMSCHMELZE GmbH & Co. Kg. Hanau, Germany) was used as the copper-based BFM with a composition of 77.4Cu-7Ni-9.3Sn-6P (wt. %). The solidus and liquidus temperatures of VZ2250 are 600°C and 630°C, respectively. The BFM was prepared to obtain the following dimensions: 18 mm x 18 mm x 30 µm. The BFM was applied on both sides of the base metals before brazing.

Brazing Process

The samples were prepared in a sandwich configuration for brazing, as illustrated in **Fig. 1 (a)**. The brazing experiments were conducted in a high vacuum furnace (Mini-Vac-II, DCP 30, Tokyo Vacuum Co., Ltd) at a low pressure of 1 x 10^{-5} Pa to avoid contamination during the brazing process. The brazing process was performed at three (3) different process parameters: 680°C/ 5 min, 710°C/5 min, and 740°C/5 min. The heating and cooling rates were set to 10°C/min to ensure full melting of the BFM to provide effective bonding for joining Cu/Porous Ni/SS304 materials. The samples were allowed to cool in the furnace during cooling below 300°C.

Microstructural analysis and Compression Test

The surfaces of all brazed samples were ground using SiC abrasive papers (grit numbers: 500, 600, and 800) by standard metallographic techniques. The ground samples were, then, using 0.05-µm alumina powder (supplied by Extec Corp. Enfield, USA) to obtain a mirror-like polished surface. An optical microscope (OM) (Olympus BX61, Japan) was used to identify the joint bonding in the brazed-polished samples. A scanning electron microscope (SEM) (Phenom ProX) was used to capture the images of the bonding joints. An energy-dispersive X-Ray spectroscope (EDS), equipped with elemental analysis software, was used to identify the contents of elements in the samples. Additionally, an Empyrean X-Ray diffractometer (XRD) (Model: PANalytical, Almelo, the Netherlands) was employed to determine the molecular structure for 2θ range of 20° - 80°. **Fig. 1 (b)** depicts a compression test done in accordance with ISO Standard 13314:2011 that was conducted by use of an Instron Universal Testing Machine 3369 equipped with Bluehill 2.0 software and fixed with a 50 kN load working in crosshead speed mode at 1 mm/min. Before the compression testing, the force and gauge length were reset to zero. The measuring device on the load automatically recorded and converted the data into assessable information. Compression testing for each brazing-process parameter was conducted with at least three (3) samples to guarantee the validity of the data.

Fig. 1 (a) Samples arrangement (sandwich configuration) in a specific clamp; (b) compression test arrangement in accordance with ISO Standard 13314:2011

RESULT AND DISCUSSION

Characterization of As-received Porous Ni

The structure of the 15-PPI porous Ni is illustrated in the optical micrographs, shown in **Fig. 2**; the images were captured for different areas for analysis. In order to determine the mass and percentage of porosity for the porous Ni based on the PPI unit, the geometrical and physical features of the porous Ni were characterized. Bidulska and co-researchers' reported various methods for evaluating the porosity [15, 16]. One of the methods, which are described in the formula can be used to compute the porosity [15]:

$$\% \text{ Porosity} = \left(1 - \frac{\rho_g}{\rho_t}\right) \text{x } 100 \quad (1.)$$

where ρ_g is the green density (g/cm^3) and ρ_t is the theoretical density (g/cm^3). The theoretical density (g/cm^3); meanwhile, can be computed by using formula given by ρ_t as follows [15]:

$$\rho_t = \frac{100}{\sum_{i=1}^{n} \frac{w_i}{\rho_i}} \quad (2.)$$

where w_i is the weight percentages of elements and additives and ρ_i is the specific weight of elements and additives. However, alternative method can be employed to obtain the porosity of porous Ni. The mass of porous Ni was measured using an analytical balance by taking three (3) value (0.343 g, 0344 g, and 0.344 g) and the average value was then calculated. Meanwhile, the pore diameter was calculated by taking four (4) measurements at three to five different areas (see **Fig. 2 (c)**). Then, the average value was computed as shows in **Table 1**. The percentage of porosity was determined using the mass-to-volume direct calculation [17].

By knowing the values of mass and volume, the porosity of the porous Ni was computed by using the following formula [17]:

$$\% \text{ Porosity} = \left(1 - \frac{M}{V.\rho_S}\right) \text{ x } 100 \quad (3.)$$

where M is the mass of porous Ni (g), V is its volume (cm^3), and ρ_s is its solid density (g/cm^3). The density of solid Ni is 8.903 g/cm^3 [18]. **Table 2** shows the % porosity of porous Ni, as obtained by using Liu and Chen methods [17].

It is evident in **Table 2** that a high value of 96.14% was obtained for the porosity of porous Ni, which can be related to the enormous size of pores in the 15 PPI porous Ni, as depicted in **Fig. 2 (c)**. A porous metal with high porosity offers a good impact energy absorption as it corroborates a uniform stress throughout the deformation; a porous metal is also capable of recovering energy efficiently [19]. In addition, the 15 PPI porous Ni is lighter in weight (lower in density) due to its hollow structure and bigger diameter interconnected of struts with hexagonal dodecahedron geometry node (see **Fig. 2 (b)**). A similar geometry and interconnected porous Ni struts have also been reported by Heo and co-researchers [7], which agrees with the 15 PPI open-cell porous Ni used in the present research. Besides, the interfacial bond between the base metals and porous Ni struts can be enhanced with a similar geometry, as reported (see **Fig. 2 (a)**) by Zhao and co-researchers [20].

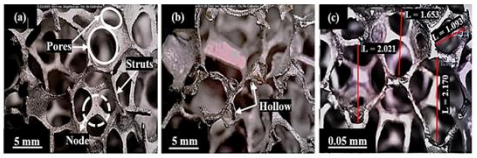

Fig. 2 Optical micrographs (from Dino-Lite microscope) showing different areas of 15-PPI porous Ni; (a) Mid part of the porous area showing hexagonal dodecahedron geometry and interconnected struts, (b) A hollow condition of the struts exposed to the cutting area, and (c) The measurement of pore diameter (in mm)

Table 1 The measurement of pore diameter (mm) as marked in **Fig. 2 (c)**

Pore diameter (mm)				Average pore diameter (mm)
Value 1	Value 2	Value 3	Value 4	
2.021	1.653	1.093	2.170	1.734

Table 2 Determination of % porosity of Porous Ni

Pore diameter (mm)	Average mass (g)	Volume (cm^3)	% Porosity
1.734	0.344	1.000	96.138

Microstructural Analysis of Brazed Cu/Porous Ni/SS304

A successful brazed joint was achieved by applying the process parameters, as stated in the experimental work (Sect. 2). The porous Ni maintains its structure; it is slightly rigid, and changes colour from grey to white as perceived by the naked eyes after brazing. This change in colour might be caused by the diffusion of BFM during brazing. The elements and possible phase transformations involved were investigated using SEM-EDS analysis. SEM micrographs for all samples are shown in **Fig. 3** and presented as two interfaces: Cu (Interface 1) and SS304 (Interface 2).

At the brazing temperature of 680°C, it can be seen the molten VZ2250 BFM effectively diffused into the porous Ni as well as into both base materials (Cu and SS304). It can be noticed in **Fig. 3** that the joining was robust, and the molten VZ2250 BFM seems to coat the joint structures. For all samples, the VZ2250 BFM diffused into the porous Ni and up to a certain depth of the base metal surfaces. A different pattern of dark grey colour can be observed in the SEM micrographs in **Fig. 3**, which signify the diffusion of the BFM on completion of the brazing process. Furthermore, the porous Ni is observed to be firmly bonded with the base metals.

The BFM is seen to have diffused more effectively towards the porous Ni as compared to base metals. It can be noticed from **Fig. 3 (a)** that the diffusion of the BFM into the porous Ni is likely to coat the porous Ni, as explained in Section 3.1; the hollow structure of the struts supports this observation. However, it can be seen in **Fig. 3 (b) and (c)**) that diffusion occurred more effectively in the porous Ni, which resulted in the voids and dendrites growth, and all these behaviours can be clearly observed at the Cu/Porous Ni interface (Interface 1) (see **Fig. 3 (a-c)**). In other words, when the brazing temperature increases, microstructure flaws like voids and cracks start to show up and the diffusion zone increases, thus inquiring about the joint's reliability at higher brazing temperatures. The brazing temperature of 680°C was found to be sufficient to result in an even diffusion of the molten VZ2250 BFM on both interfaces (Interface 1 and Interface 2) as compared to the brazing temperatures of 710°C and 740°C.

Further analysis was done using SEM-EDS to analyses the elemental composition at both interfaces. It is interesting to focus on the sample brazed at 680°C/5 min because this sample corresponds to the least void areas. **Table 3** shows the elemental composition at different points for both interfaces, which is in accordance with **Fig. 3 (a, d)**.

It is evident in **Table 3** that nickel (Ni) was capable of diffusing at all points, except at points 1, 2, and 11; similarly, phosphorus (P) was able to diffuse at all points, except at points 5, 9, and 12. In general, nickel and phosphorus were capable of diffusing at most of the points. For both interfaces, nickel and phosphorus exhibit the highest elemental compositions (at. %) along the porous Ni area (see **Table 3**). These results show that the VZ2250 BFM tends to coat the porous Ni. The high nickel and phosphorus contents indicate that nickel and phosphorus (dark grey mixed white colour) originate on the coated area (points 3, 6, 7, and 8) to form a diffusion layer during brazing. Besides, phosphorus dissolves well in porous Ni, which causes them to diffuse [21]. Therefore, it is believed that the brazing temperature of 680°C exhibits the BFM migration through the porous Ni struts (**Fig. 2 (a)**) thereby coating certain areas of the porous Ni structure. Meanwhile, the light grey colour at the diffusion zone area indicated the enrichment with copper and tin (Sn) by spotting at points 2 and 11, and Sn was found near the end side of porous Ni, which can be seen in points 6 and 8. Tin was believed to have readily diffused from the VZ2250 BFM into porous Ni because Sn is a low melting-temperature metal and it is an active element, as well [22]. Tin and copper form a possible solid-solution phase of Cu-Sn. It is, therefore, quite logical to conclude that the Cu-P and Cu-Sn phases tend to form a strong joint.

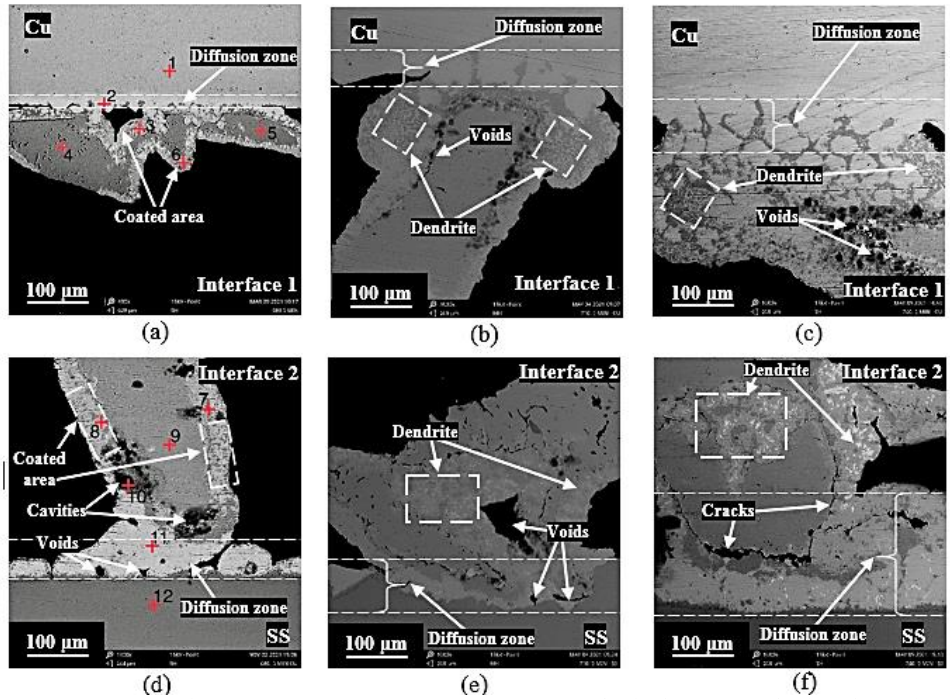

Fig. 3 SEM micrographs for various brazing process parameters: (a) & (d) 680°C/5 min, (b) & (e) 710°C/5 min, and (c) & (f) 740°C/5 min. Images (a) – (c) are for Interface 1, and (d) – (f) for Interface 2. SS = stainless steel 304

Table 3 Compositions at different points for 680°C/5 min as marked in **Fig. 3 (a)** for Interface 1 and **Fig. 3 (d)** for Interface 2

Interface	Point	Elemental composition (at. %)							Possible Phase/Area
		Cu	Ni	Sn	P	Fe	Mn	Cr	
1	1	99.10	0.43	0.20	0.27	-	-	-	Cu – base metal
	2	89.21	4.19	4.27	1.67	0.27	0.33	0.05	Cu-Ni-Sn / Cu-Sn
	3	64.96	25.94	2.99	6.03	-	-	0.08	Cu-Ni / Cu-P
	4	7.14	91.86	0.06	0.13	0.75	-	0.06	Ni – porous Ni
	5	-	99.52	0.01	-	-	0.25	0.22	Ni – porous Ni
	6	3.79	70.68	6.52	18.45	-	0.56	-	P-Sn / Ni-P
2	7	-	73.86	0.52	25.33	0.11	-	0.17	Ni-P
	8	6.59	68.78	6.31	18.02	0.14	0.16	-	Ni-P
	9	0.53	99.47	-	-	-	-	-	Ni – porous Ni
	10	20.61	54.63	-	24.11	0.30	-	0.34	Cu-Ni / Ni-P
	11	92.91	0.54	4.93	0.77	0.86	-	-	Cu-Sn
	12	0.24	9.05	0.14	-	69.57	1.93	19.08	SS304 – base metal

Interface Analysis of Cu/Porous Ni/SS304

It has been established in Sect. 3.2 that the VZ2250 BFM effectively diffused on both sides of Cu/Porous Ni and Porous Ni/SS304 interfaces during brazing at various temperatures. The interfacial reaction resulted in the formation of intermetallic compounds. It was observed that there is no apparent phase change occurred at either brazed Interface 1 or 2 for all samples. Therefore, a selected sample was further analyzed by using XRD. The presence of inter-metallic compounds in the brazed joint was investigated for the sample brazed at 680°C/5 min. **Fig. 4** shows the XRD analysis at both interfaces. The same phases (Cu_6Sn_5 and Cu_3P) have been discovered in Interface 1 (Cu/Porous Ni) in a similar study using BFM (77.6Cu-5.7Ni-9.7Sn-7P) brazed with Cu/Porous Cu [20]. However, studies on Interface 2 (Porous Ni/SS304) are rarely found for comparison.

It can be seen in **Fig. 4 (a)** that the elements Cu, Sn, and P dominated the peak with the highest intensity. It was also noticed that the following solid-solution phases influenced the phase transformation at Interface 1: Cu-Ni-Sn, Cu-Sn, Cu-P, Ni-Sn, and P-S. In particular, the inter-metallic compound Cu_6Sn_5 at 2θ of 43.01°, 50.30°, 52.28°, 74.15°, and 76.70° and P_3Sn at 2θ of 44.92°, 50.30°, 52.28°, 74.15°, and 52.28° has become a dominant peak as all Cu_6Sn_5 and P_3Sn peaks overlapped arose. Meanwhile, the Cu_3P arose at 2θ of 43.01°, 44.92°, and 52.28°, which are the same as those in the XRD peak pattern.

In the meantime, Cu, Ni, Sn, P, Fe, and Mn dominated the peak with the highest intensity in **Fig. 4 (b)**. It was also discovered that Cu-Sn, Fe-Mn-Ni, Fe-Ni-P, Fe-Ni, Mn-Ni, and Ni-Sn containing phases influenced the phase transformation at Interface 2. Most of these peaks arose at 2θ of 42.79°, 44.71°, 52.08°, 74.72°, and 76.51°, which is the same in the XRD peak pattern

list of $Cu_{20}Sn_6$ and $Fe_{1.2}Ni_{0.9}P$, has becomes to be dominating peaks. The SS304 base metal and VZ2250 BFM contribute to the presence of these phases. Besides, the $Cu_{20}Sn_6$ phase is formed when Sn diffuses into Cu, and it tends to increase the tensile strength of the material [23]. Additionally, $Fe_{0.5}Mn_{0.2}Ni_{0.3}$ peak then arose at 2θ of 43.61°, 50.78°, and 74.42°, and the brittle phase $MnNi_3$ [24] arose at 2θ of 43.61°, 5078°, and 74.72°.
To summarize, it is validated by EDS point analysis that the elements, that could diffuse into the base metals (Cu and SS304) and porous Ni, tend to form inter-metallic compounds during brazing with the VZ2250 BFM. The EDS observations agreed with the XRD results. The completely molten VZ2250 BFM had a homogeneous chemical composition and infiltrated the pore spaces in between the struts of porous Ni (**Fig. 3 (a)**) via capillary action [21]. Besides this, nickel and phosphorus in the VZ2250 BFM diffused into the base metals (Cu and SS304) and porous Ni due to the concentration gradient to form the diffusion layer [25]. Furthermore, some of the phosphorus will evaporate due to its high vapour properties [26] and emerge in enriching copper and tin mostly in the porous Ni area, which resulted in the formation of brittle phases: Cu_3P and Cu_6Sn_5 [22, 26]. The Cu_3P and Cu_6Sn_5 in the BFM have melted and coalesced with the porous Ni and base metal to form a strong and comparatively brittle joint.

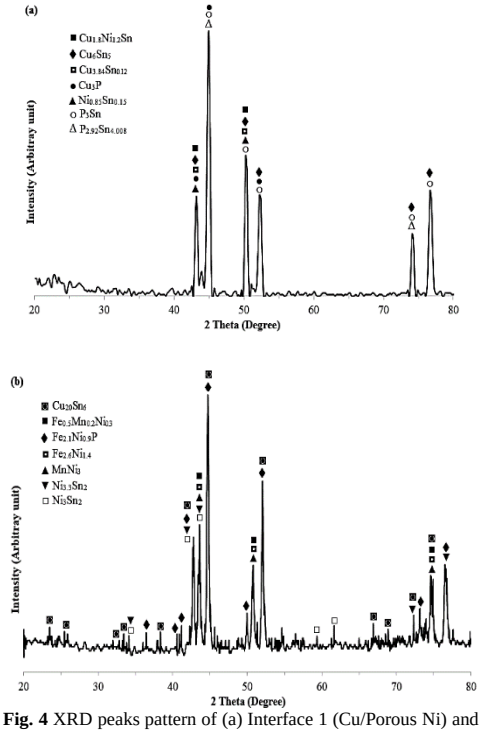

Fig. 4 XRD peaks pattern of (a) Interface 1 (Cu/Porous Ni) and (b) Interface 2 (Porous Ni/SS304)

Compressive Strength Analysis of Brazing Cu/Porous Ni/SS304

Compression tests were conducted to investigate the effects of brazing process parameters on the rigidity of porous Ni. The compressive strength can be related to the extent of diffusion of BFM into the porous Ni during brazing; it can also be related to the post-welding microstructural evolution in the porous Ni. **Fig. 5** presents the column chart showing the compressive strengths of the brazed Cu/Porous Ni/SS304 and non-brazed Cu/Porous Ni/SS304 samples at various brazing temperatures. The non-brazed Cu/Porous Ni/SS304 condition refers to porous Ni only. The compression-test results show that the compressive strength declines linearly with the increase in the brazing temperature from 680°C to 740°C; it is encouraging to note in **Fig. 5** that the maximum compressive strength of 15.75 MPa is achieved at the brazing condition of 680°C/5 min. Besides this, the post-brazed porous Ni structure shows a higher compressive strength than the non-brazed condition. Since the highest maximum compressive of around 16 MPa is achieved by brazing at 680°C/5 min, it can be concluded that the molten VZ2250 BFM has effectively and evenly diffused into the struts at the specified brazing condition. The lower compressive strengths of brazed Cu/Porous Ni/SS304 at higher brazing temperatures can be justified in view of the microstructures observed in **Fig. 3 (b, c, e, and f)**. It is evident in **Fig. 5** that the compressive strengths of brazed Cu/Porous Ni/SS304 samples are much higher as compared to the compressive strength of the non-brazed sample. Brazing of Cu/Porous Ni/SS304 using VZ2250 BFM enhances the former's compressive strength, which is justifiable due to the BFM coating on the porous Ni struts (see **Fig. 3 (a, d)**). In order to observe the condition of both interfaces after the compression strength test, the compressed porous Ni regions were manually removed from the tested sample. The images in **Fig. 5** show the conditions of the samples at both interfaces. The left-over porous Ni region that covered the Cu interface at the brazing temperature of 680°C can be observed in **Fig. 5 (a)**; here most of the porous Ni is seen to be in contact with the Cu, based on the remaining BFM residue. It was difficult the removal of the compressed porous regions, as the structure was sturdy. This difficulty in the removal of the compressed porous regions indicates that the joining between the porous Ni and Cu interface at the brazing temperature of 680°C is relatively strong. However, brittle fractures of some porous Ni regions occurred during the removal process, which is indicated as missing regions in **Fig. 5 (b – c)**. The observations of images 5 (d, e, f) depict that the left-over porous Ni region has covered the SS304 interface. For brazing temperatures of 680°C and 710°C, the microstructural features of porous Ni contact and the SS304 are closely comparable (see **Fig. 5 (d, e)**), but they differ so for brazing temperatures of 740°C. The SS304 (Interface 2) braze-joint breaking process is likely similar to the Cu (Interface 1); as the brazing temperature increases, the joint becomes more brittle.
These findings lead us to conclude that the data in **Fig. 5** conforms to the analysis in **Fig. 3** and **4**. After brazing, the BFM elements react with the base metal and porous Ni to form a coated layer that is then adhered to the porous Ni struts (see **Fig. 3 (a, d)**). This layer has Cu-P and Cu-Sn phases at Interface 1 and Mn-Ni phase at Interface 2. These phases are believed to contribute to the porous Ni structure being more rigid and subsequently increase the value of compressive strength. However, as the brazing temperature increases, the roughness of the Cu-P, Cu-Sn, and Mn-Ni phases causes voids and cracks to form along the porous Ni junction between the brazed at Interface 1 (see **Fig. 3 (b)** and **(c)**) and the diffusion zone of the brazed at Interface 2 (**Fig. 3 (e)** and **(f)**), hence decreasing the value of the compressive strength.
The compressive stress-strain curves for the brazed and non-brazed samples of Cu/Porous Ni/SS304 are shown in **Fig. 6 (a)**. The initial deformation behaviour, at smaller loads during the compression test, is illustrated in **Fig. 6 (b)**, which indicated elastic deformation behaviours in both brazed and non-brazed

Cu/Porous Ni/SS304 samples; however, the deformation becomes plastic when excessive stresses are applied during the mechanical test. Mohd Zahri and co-researchers (2019) have reported that there occurs a pores-size reduction in the porous Ni (for both brazed and non-brazed conditions) when the compressive stresses surpass the yield strength of the cell wall [22].

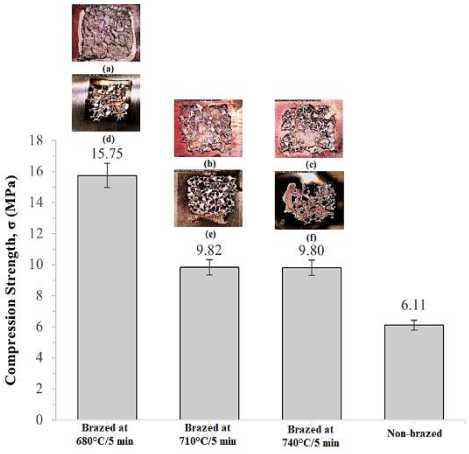

Fig. 5 Compressive strength of brazed and non-brazed Cu/Porous Ni/SS304 condition with images of (a) – (c) the condition of residue porous Ni at the Cu interface and (d) – (f) the condition of residue porous Ni at the SS304 interface after brazing.

The stress-strain curves in **Fig. 6** indicate that the deformation behaviour in brazed and non-brazed Cu/Porous Ni/SS304 samples are almost similar. The ductility of the brazed Cu/Porous Ni/SS304 condition is reflected in the extended plateau region (from point A to point B). The elastic curve of the brazed Cu/Porous Ni/SS304 in **Fig. 6 (b)** shows a broader strain (ε_{cr}) range. This deformation behaviour was probably caused by the VZ2250 BFM elements' atoms that effectively diffused into the porous Ni thereby contributing to the strengthening of the porous Ni structure, especially at a brazing temperature of 680°C, which is reflected in the greater area under the curve in the elastic region, as compared to the samples brazed at 710°C and 740°C, and in non-brazed Cu/Porous Ni/SS304 condition.

The dramatic rise in the curve at point B (**Fig. 6 (a)**) indicated that there occurred a collapse of the porous Ni struts, which may be attributed to the continual deformation beyond the plateau stress (σ_{pl}) point; this deformation behaviour is in agreement with the literature [21]. This stage is known as densification; here the density of the porous Ni increases to its maximum level because the cell wall eventually collapses as the porous Ni fully compacts. Now, the smooth and long plateau region, in the stress-strain curve, is considered; this region for the non-brazed Cu/Porous Ni/SS304 sample exhibits ductile behaviour under stress that is essentially constant. This research findings can be scientifically justified as follows. The non-brazed Cu/Porous Ni/SS304 sample can continued to absorb the energy during loading even though it was in a state of compressive deformation. In addition, the compressive stress-strain curve also demonstrates the ability of 15 PPI porous Ni to absorb the excess energy due to its high-stress amplitude.

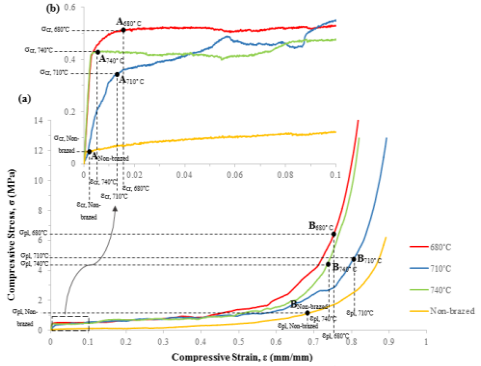

Fig. 6 (a) Compressive stress-strain curves for brazed and non-brazed Cu/Porous Ni/SS304, and (b) inset compressive stress-strain curves at 0 – 0.1 σ.

CONCLUSIONS

This research presented the characterisation of brazing porous Ni to Cu and SS304 using VZ2250 BFM. The characteristics of the joint interfaces were analysed, and the compressive strength and fracture surface around the joint interfaces were evaluated. The EDS analysis showed high nickel and phosphorus contents (at. %) in the porous Ni area for both interfaces: Cu (Interface 1) and SS304 (Interface 2). It was discovered that the brittle phases of Cu_3P and Cu_6Sn_5 were formed at Interface 1 and $MnNi_3$ for Interface 2, respectively. The diffusion of phosphorus into porous Ni has contributed significantly by their fluidity, structure of porous Ni (interconnected struts), capillary action, and concentration gradient. The maximum compressive strength of 15.75 MPa for Cu/Porous Ni/SS304 was recorded for brazing at 680°C/5 min. On the hand, a low compressive strength (6.11 MPa) was observed for non-brazed sample. The high compressive strength is attributed to the diffusion of the BFM into the porous Ni during brazing. Brittle phases were detected at porous areas near the brazed interfaces. However, the increasing brazing temperature compromised test and manually removing the compressed porous Ni, it was observed that more left-over porous Ni remained at the base metals. This condition proves the good bonding of the brazed joints. For future works, it is planned to further test the bonding strength at both interfaces so the value of bonding strength can be obtained for better identification of suitable applications.

Acknowledgements: All the authors are grateful for support provided by the Universiti Malaya Research University Grant (RU Faculty) Project number: GPF063A-2018. The authors also acknowledge Azbil Corporation and Tokyo Radiator for providing part of the research materials.

REFERENCES

1. Y. Wu, Y.Wang, R. Liu, X. Feng: Chemical Engineering Research and Design, 165, 2021, 150-161. https://doi.org/10.1016/j.cherd.2020.10.023.
2. P. Kapustenko, S. Boldyryev, O. Arsenyeva, G. Khavin: Journal of Cleaner Production, 17 (10), 2009, 951-958. https://doi.org/10.1016/j.jclepro.2009.02.005.
3. O. Stepanov, N. Rydalina, E. Antonova: The use of porous metals in heat exchangers, IOP Conference Series: Materials Science and Engineering, 890, 2020, 012150. https://doi.org/10.1088/1757-899X/890/1/012150.
4. S-F. Fan et al.: Transactions of Nonferrous Metals Society of China, 27 (1), 2017, 117-124. https://doi.org/10/1016/S1003-6326(17)60013-X.

5. N. Michailidis et al.: Solar Energy Materials and Solar Cells, 109, 2013, 185-191. https://doi.org/10/1016/j.solmat.2012.10.021.
6. H. Sabetghadam, A. Z. Hanzaki, A. Araee: Materials Characterization. 61 (6), 2010, 626-634. https://doi.org/10.1016/j.matchar.2010.03.006.
7. H. Heo et al.: Materials Science and Engineering: A, 740-741, 2019, 63-70. https://doi.org/10/1016/j.msea.2018.10.022.
8. J. Deng et al.: Materials Today Communications, 28, 2021, 102544. https://doi.org/10/1016/j.mtcomm.2021.102544.
9. V. Mangla, J. D. Sharma, S. Kumar, P. D. Kumar, A. Agarwal: Materials Today: Proceedings, 26, 2020, 724-727. https://doi.org/10/1016/j.matpr.2020.01.016.
10. T. Suga et al.: Welding International, 30 (3), 2016, 166-174. https://doi.org/10.1080/09507116.2014.921090.
11. H. Ren, X. Ren, W. Long, B. Chen, S. Pang, H. Xiong: Progress in Natural Science: Materials International, 31 (2), 2021, 310-318. https://doi.org/10.1016/j.pnsc.2020.12.009.
12. S. Chen, J. Huang, J. Xia, H. Zhang, X. Zhao: Metallurgical and Materials Transactions A, 44 (8), 2013, 3690-3696. https://doi.org/10.1007/s11661-013-1693-z.
13. X. Yuan, K. Tang, Y. Deng, J. Luo, G. Sheng: Materials & Design (1980-2015), 52, 2013, 359-366. https://doi.org/10/1016/j.matdes.2013.05.057.
14. GH Induction Atmosphere, The brazing guide. https://www.ghinduction.com/wp-content/uploads/2011/09/GH-Brazing-Guide1.pdf, 2011 (accessed on 22 March 2022).
15. J. Bidulská, T. Kvačkaj, I. Pokorný, R. Bidulský, M. Actis Grande: Archives of Metallurgy and Materials, 58 (2), 2013, 371-375. https://doi.org/10.2478/amm-2013-0002.
16. J. Bidulská, R. Bidulský, M. Actis Grande, T. Kvačkaj: Materials, 12 (22), 2019, 3724. https://doi.org/10.3390/ma12223724.
17. P.S. Liu, G.F. Chen: Chapter Nine – Characteristics methods: basic factors, first ed., Butterworth-Heinemann, 2014.
18. F. C. Campbell: Elements of Metallurgy and Engineering Alloys, ASM International ed., Ohio, USA, 2008.
19. A. N. M. Alhusseny, A. Nasser, N.M. J. Al-Zurfi: High Porosity Metal Foams: Potential, applications, and formulations, Porosity – Process, Technologies and Applications. InTech, 2018. https://doi:10.5772/intechopen.70451.
20. L-Z. Zhao, M-J. Zhao, N. Li, H. Yan, J-S. Zhang: Transactions of Nonferrous Metals Society of China, 20, 2010, s463-s466. https://doi.org/10.1016/S1003-6326(10)60519-5.
21. N. A. M. Zahri et al.: Welding in the World, 64, 2020, 209-217. https://doi.org/10/1007/s40194-019-00804-2.
22. N. A. M. Zahri, F. Yusof, T. Ariga, A. S. M. A. Haseeb, M. A. Mansoor, N. L. Sukiman: Materials Science and Technology, 35, 2019, 2004-2012.
23. S. E. Susilowati, D. Sumardiyanto: International Journal of Metallurgical Engineering, 6 (1), 2017, 10-17. https://doi:10.5923/j.ijmee.20170601.02.
24. V. V. Bannikov, I.R. Shein, A. L. Ivanovskii: Physica B: Condensed Matter, 405 (22), 2010, 4615-4619. https://doi.org/10.1016/j.physb.2010.08.046.
25. P. L. Zhang, S. Yao, M. Ding, F. G. Lu, S. N. Lou: International Journal of Materials Research, 101, 2010, 1436-1440. https://doi.org/10.3139/146.110376.
26. Z. Zhong, J. Zhao, X. Shen, X. Ling: Welding Journal, 91 (9), 2012, 237s-240s.